A study on PDC drill bits quality

Malik Yahiaoui, Laurent Gerbaud, Jean-Yves Paris, Jean Denape, Alfazazi Dourfaye

A study on PDC drill bits quality

M. Yahiaoui [a,*], L. Gerbaud [b], J.-Y. Paris [a], J. Denape [a], A. Dourfaye [c]

[a] Laboratoire Génie de Production, Université de Toulouse, Ecole Nationale d'Ingénieurs de Tarbes, 47 avenue d'Azereix 65016 Tarbes, France
[b] Centre de Géosciences, Mines Paritech, France
[c] Varel Europe, France

Keywords:
PDC cutters
Wear rate
Quality factor
Cobalt carbide
Residual stresses
Leaching

A B S T R A C T

The quality of innovating PDC (Polycrystalline Diamond Compact) bits materials needs to be determined with accuracy by measuring cutting efficiency and wear rate, both related to the overall mechanical properties. An original approach is developed to encompass cutting efficiency and wear contribution to the overall sample quality. Therefore, a lathe-type test device was used to abrade specific samples from various manufacturers. Post-experiment analyzes are based on models establishing coupled relationships between cutting and friction stresses related to the drag bits excavation mechanism. These models are implemented in order to evaluate cutting efficiency and to estimate wear of the diamond insert. Phase analysis by XRD and finite element simulations were performed to explain the role of physicochemical parameters on the calculated quality factor values. Four main properties of PDC material were studied to explain quality results obtained in this study: cobalt content in samples that characterizes hardness/fracture toughness compromise, undesired phase as tungsten carbide weakening diamond structure, diamond grains sizes and residual stresses distribution affecting abrasion resistance.

1. Introduction

The main tools employed in the drilling industry are roller cone and drag bits. Roller cone bits work by impact excavation and are currently used in hard rock formations because of a convenient wear resistance. Drag bits rather operate by shear mode in softer rock to medium hard formations. Nevertheless, they suffer from thermal abrasive wear and impact damage while drilling interbedded formations. As excavation rate is directly related to the overall cost, the drag bits using PDC (Polycrystalline Diamond Compact) cutters are really attractive compared to roller cone bits. In fact, PDC bits could drill twice faster and longer than roller bits even in hard formations [1]. Petroleum and hydrothermal investigations in deep geological formations lead to manufacturing new bits materials able to drill at higher temperature, in more abrasive and harder geological fields. Such innovating materials, sintering processes and design, recently developed to improve drill bits hardness and fracture toughness, also require new strategies in quality assessment. Drag bits are mostly damaged by abrasion [2] and thus quality can be defined by two main parameters: materials wear rate and excavation performance. Wear rate calculus by Archard's model has been commonly used in several works to describe PDC/rock behavior [3]. Excavation performance depends on cutting efficiency which is initially determined by the sample depth of cut. During friction, cutting efficiency evolves and the change is closely linked to wear flat formation on PDC cutters. Because a long bit life could be related to a poor cutting performance and vice versa, this paper proposes an objective quality criterion to clearly classify PDC cutters. Drilling mechanisms and material analyzes are taken into consideration to interpret the grading of the testing bits.

2. PDC samples

Six cutters coming from various manufacturers (referred from A to F) were selected to represent a large range of properties. Cutters are made of a tungsten carbide cylinder surmounted by a diamond table (Fig. 1a). Material parts have a diameter of 13 mm: the tungsten carbide cylinder has a height of 8 mm and the diamond layer is around 2 mm thick. Diamond tables have a chamfer of $45^\circ \times 0.4$ mm except for sample C where it is $45^\circ \times 0.7$ mm. These cutters were sintered by HPHT (i.e. High Temperature and High Pressure) at a temperature over 1400 °C under a pressure close to 5.5 GPa (Fig. 1b) [4].

Tungsten carbide prismatic grains in a binder cobalt phase form the substrate part (Fig. 2a). The mean grain size of tungsten carbide is around 2 μm with minimum and maximum values observable under

* Corresponding author. Tel.: +33 5624 42700; fax: +33 5624 42708.
E-mail addresses: malik.yahiaoui@enit.fr, yahiaouimalik@gmail.com (M. Yahiaoui).

http://dx.doi.org/10.1016/j.wear.2012.12.026

Nomenclature

α	back rake angle, deg
ε	intrinsic specific energy, J m^{-3}
η	cutting efficiency
μ	friction coefficient
ρ_x	cobalt mass content at distance x
ζ	cutting coefficient
A_c	cross-sectional area of cut, m^2
A_f	wear flat area, m^2
D	infiltration coefficient, m^2 s^{-1}
E	specific energy, J m^{-3}
E_0	initial specific energy, J m^{-3}
E_m	cutting dissipated energy, J
F^c	cutting force component, N
F^f	friction force component, N
F_N	total normal force, N
F_N^0	initial normal force, N
F_T	total drag force, N
G	grinding ratio
I	sum of maximum peak of present phases
I_{CoC_x}	CoC_x XRD maximum peak intensity
$I_{diamond}$	diamond XRD maximum peak intensity
I_{WC}	WC XRD maximum peak intensity
k	wear rate, m^3 N^{-1} m^{-1}
L	excavation distance, m
L_T	total excavation distance, m
Q	quality factor
R^2	coefficient of determination
t	time of infiltration, s
u	cutting capacity, m
V_C	cutter worn volume, m^3
V_R	cut rock volume, m^3
W_m	cutter mechanical work, J
x_i	infiltration transition position, m

a micrometer and over 10 μm (Table 1). Jeol JSM-7000F field emission scanning electron microscope observations revealed aggregates of micrometric diamond grains also surrounded by cobalt (Fig. 2b). Samples A, E and F have been exposed to a chemical post-treatment called "leaching process" [5]. This treatment removes interstitial cobalt grain boundaries on the diamond layer beyond several tens of micrometers (Fig. 2c).

The cobalt phase in the diamond part is due to the infiltration of cobalt from the tungsten carbide substrate during sintering. Commonly, cobalt proportion can represent 6–18 wt.% in tungsten carbide substrate and 2–8 wt.% in the diamond part. The cobalt distribution in samples follows a law that can be expressed as a solution [6] of differential equations from Fick's laws (Eq. (1)).

$$\rho(x) = (\rho_0 - \rho_{10}) \frac{\operatorname{erfc}\left[\frac{1}{2\sqrt{D \cdot t}}(x - x_i)\right]}{\operatorname{erfc}\left[-\frac{1}{2\sqrt{D \cdot t}}x_i\right]} + \rho_{10} \quad (1)$$

In this equation, $\rho(x)$ represents axial cobalt mass content from diamond face (where $\rho(x) = \rho_0$) to the bottom of the tungsten carbide part (where $\rho(x) = \rho_{10}$). D is the infiltration coefficient, t is the time of infiltration and x_i expresses infiltration transition position between PDC and WC-Co materials. The cobalt

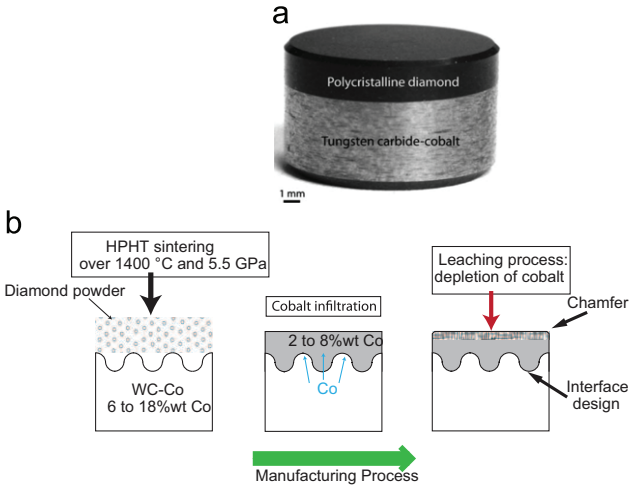

Fig. 1. PDC cutter: (a) photography of a cutter; (b) manufacturing process of a cutter.

distribution was measured on the samples (Fig. 3) using energy dispersive X-ray spectrometry (EDX) analyzes with Bruker XFlash 4010 detector. To perform semi-quantitative measurements, the detector was calibrated with copper located close to samples before each observation campaign. For these measurements, the six samples were longitudinally cut by electroerosion, polished and metalized with palladium. The SEM was adjusted at 15 kV with a working distance of 15 mm. The electron beam intensity was set around 100 counts per second to enable a high speed analysis. The cobalt mass content distribution was evaluated with a step of 500 μm along a line on sections.

EDX characterizations showed that all samples have similar cobalt content (ρ_0) around 3 wt.% in the diamond material whereas cobalt content of tungsten carbide (ρ_{10}) part can vary from 8 to 17 wt.% (Table 2). The square root of $D \cdot t$ permits to evaluate dispersion of the inflection i.e. metal ability to spread from tungsten carbide to diamond. D depends on diamond/WC grains size and on sintering temperature. At sintering temperature, molten cobalt moves by capillarity through voids between diamond grains. Larger voids are directly associated with larger grain size which favors displacement of cobalt [7]. Moreover, metal infiltration in diamond structures increases with temperature as viscosity of molten cobalt decreases.

SEM observations only permit the measurement of diamond aggregates (see Table 1). The aggregates size does not represent the diamond grain size distribution in the sample and cannot be directly related to the mechanical behavior of PDC materials. Considering that t is almost equal for the six samples, $\sqrt{D \cdot t}$ parameter permits to qualitatively evaluate diamond grain sizes rather than of aggregate ones. Here, B and C displays $\sqrt{D \cdot t}$ values two times higher than those of samples A, D, E and F. Theses results may be due to higher diamond grain sizes in samples B and C than in the others.

3. Experimental study

A vertical lathe-type device was used to simulate drilling conditions. Cutters brazed on sample holders were adjusted downward on the lathe shaft. Ring-stone counter-faces were made of a manufactured mortar rock (1 m in external diameter, 0.5 m in internal diameter and 0.6 m thick with a density of 2210 kg m^{-3}). This mortar ensures homogeneous chemical composition (silica content of 80 wt.%) and mechanical properties

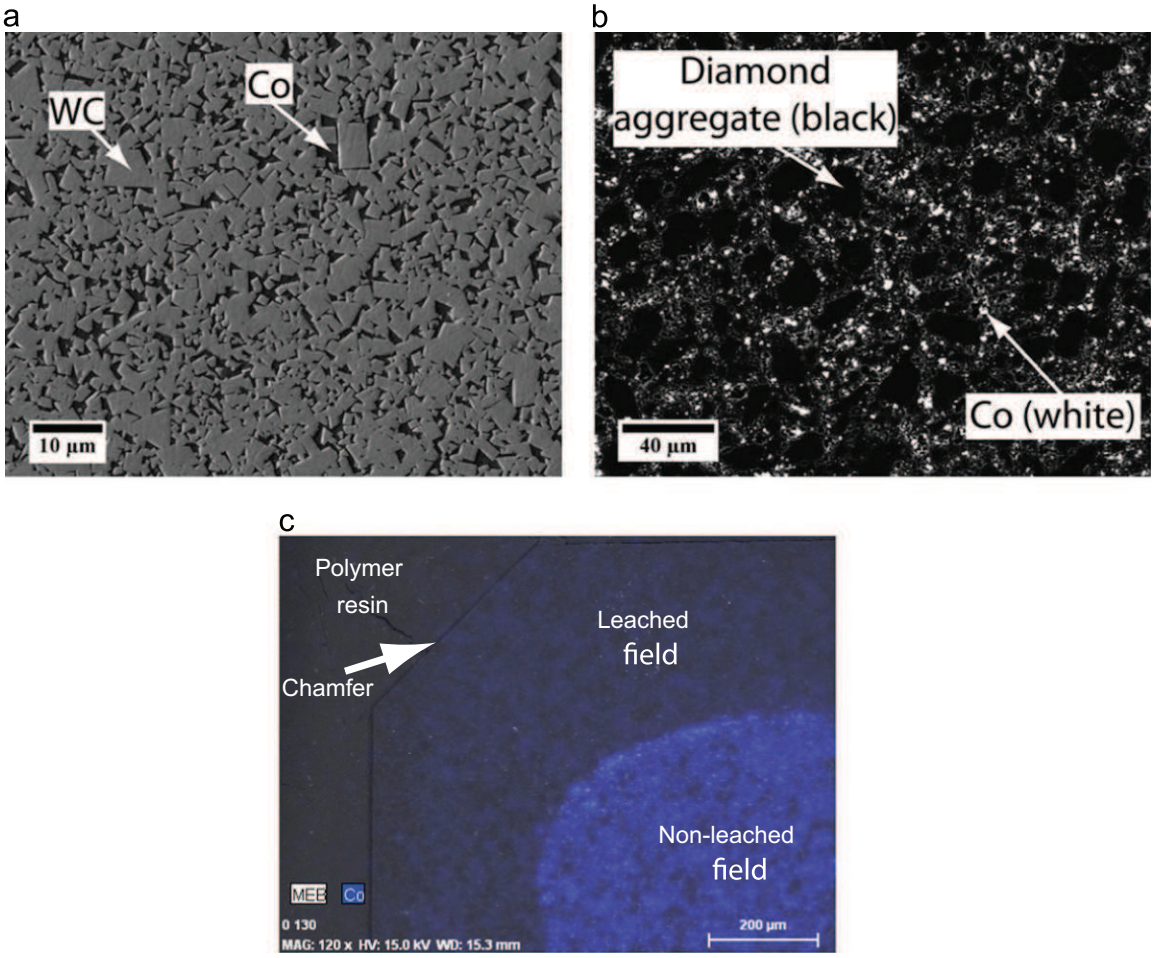

Fig. 2. SEM images at 15 kV: (a) sample B tungsten carbide-cobalt part by secondary electron analysis; (b) sample B diamond part by backscattered electron analysis; (c) illustration by secondary electron and colorized energy dispersive X-ray spectrometry (EDX) mapping of cobalt leaching zone for sample F. (For interpretation of the references to color in this figure legend, the reader is referred to the web version of this article.)

Table 1
Geometry and microstructural properties of PDC samples A to F measured by SEM image analysis.

Cutters	A	B	C	D	E	F
Section view 8.3 × 6.2 mm	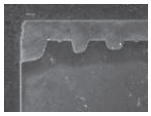	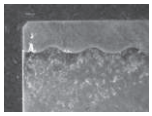	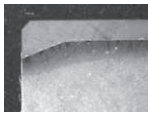	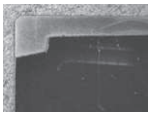		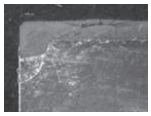
Side diamond thickness (mm)	2.3 ± 0.05	1.6 ± 0.05	2.1 ± 0.05	2.4 ± 0.05	2.0 ± 0.05	2.1
Diamond aggregate size (µm)	13.3 ± 3.9 min < 4.5 max > 21.8	15.1 ± 5.8 min < 7.2 max > 29.9	9.8 ± 4.8 min < 3.1 max > 23.8	8.1 ± 5.1 min < 2.3 max > 20.5	11.6 ± 4.6 min < 3.2 max > 21.4	11.0 ± 5.0 min < 3.4 max > 22.4
WC-Co grain size (µm)	2.5 ± 1.1 min < 0.8 max > 5.7	1.9 ± 1.7 min < 0.3 max > 9.8	2.0 ± 1.3 min < 0.5 max > 8.3	1.4 ± 1.1 min < 0.4 max > 9.1	1.7 ± 1.0 min < 0.5 max > 6.2	2.2 ± 1.1 min < 0.3 max > 7.0
Leaching depth (µm)	70 ± 4	–	–	–	~100[a]	325 ± 30

[a] Not measured, manufacturer data.

(compressive strength of 21.6 MPa and young modulus of 48.1 GPa). Experiments were carried out according to real drilling conditions (Fig. 4a): normal load ranged from 3000 to 5000 N, back rake angle at 15°, penetration depth of 2 mm and mean cutting speed of 1.8 m s^{-1}. Tests were conducted in atmospheric environment and no lubricant was added into the contact.

Experiments were performed following four sequences on the mortar ring and each sequence represents three radial round-trips (i.e. an excavation length about 510 m). As a consequence, one mortar ring works for a total length of 25 500 m. At the end of each sequence, the height of material lost was measured to calculate cutting active area A_c and cutter worn volume V_c.

4. Wear rate analysis

PDC drill bits are made of tens of cutters (e.g. VTD616 tools from Varel International have 48 face cutters). Operating

parameters as weight and torque on bit, defined for a constant penetration speed, could be considered as independent of the number of bits [8]. This condition is assumed by a correct cutters repartition on the bit, which ensures a homogenized wear on every PDC [9]. Therefore, wear behavior and drilling performance information based on single cutter experiments are relevant and can be extrapolated to understand the whole tool behavior. Afterward, Fairhurst and Lacabanne [10] assume that cutting action and sliding friction can also be considered as independent (Eq. (2)) in the drilling procedure (Fig. 4). Thus, normal force F_N applied onto a cutter can be expressed as the sum of friction normal force F_N^f and cutting normal force F_N^c. Moreover, an approximation of F_N^f can be expressed as the difference between normal force applied to a cutter and initial value of the normal force, noted as F_N^0

$$F_N = F_N^f + F_N^c \approx F_N^f + F_N^0 \tag{2}$$

The same approach is assumed for the transverse force F_T, so that (Eq. (3))

$$F_T = F_T^f + F_T^c \approx F_T^f + F_T^0 \tag{3}$$

Because this study is clearly a case of abrasive friction between cutter and hard rock, Archard's model is an interesting choice. This model has been extensively involved in tribological studies because of its simple linear relationship (Eq. (4)) between wear volume V_c and the product of the normal force F_N^f by the sliding distance L (Fig. 5a)

$$V_c = k \cdot F_N^f L \approx k \cdot (F_N - F_N^0) L \tag{4}$$

The coefficient of proportionality k is usually called wear rate and could be expressed as a function of rock or cutter hardness, but only proportionality is considered here, and its meaning is not identified.

Wear rate calculations show that cutter A gives the best wear behavior with a rate value lower than 1×10^{-8} mm^3 N^{-1} m^{-1}, while cutter B obtains the highest rate value over 16×10^{-8} mm^3 N^{-1} m^{-1} (Fig. 5b).

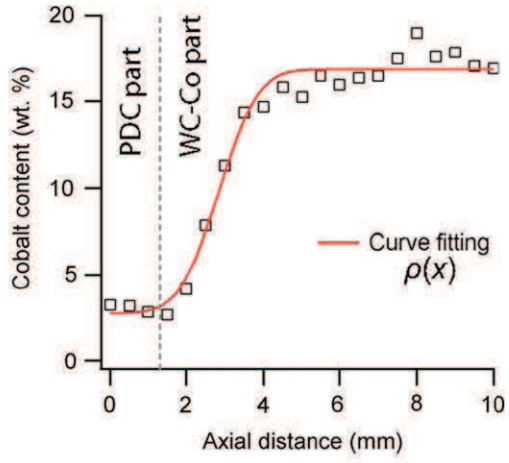

Fig. 3. EDX longitudinal measurement of cobalt content from diamond to tungsten carbide material for sample B.

5. Cutting capacity

Detournay and Defourny [11] established a linear relationship between torque on cutter (i.e. F_T) and weight on cutter (i.e. F_N). This equation involves three constant parameters ε, μ and ζ which are respectively the intrinsic specific energy, the friction coefficient and the cutting coefficient (Eq. (5)). The friction coefficient represents the ratio between the transversal and normal friction forces. The cutting coefficient is calculated by the ratio of the normal cutting component on the transversal one. The intrinsic specific energy is defined by the ratio between the normal cutting force and the cutting active area A_c. This parameter has the dimension of a stress and can be related to the strength of the rock toward the cutting action.

$$F_T = \mu F_N + A_c(1 - \mu\zeta)\varepsilon \tag{5}$$

Moreover, specific energy E represents the dissipated energy E_m needed to cut a unitary volume of rock V_R. The energy E_m equals the transverse force F_T multiplied by the cutter travel distance L. The lateral displacement of the tool front face implies that dug volume V_R equals the product of active area A_c by distance L. As a consequence, F_T and A_c measurements permit

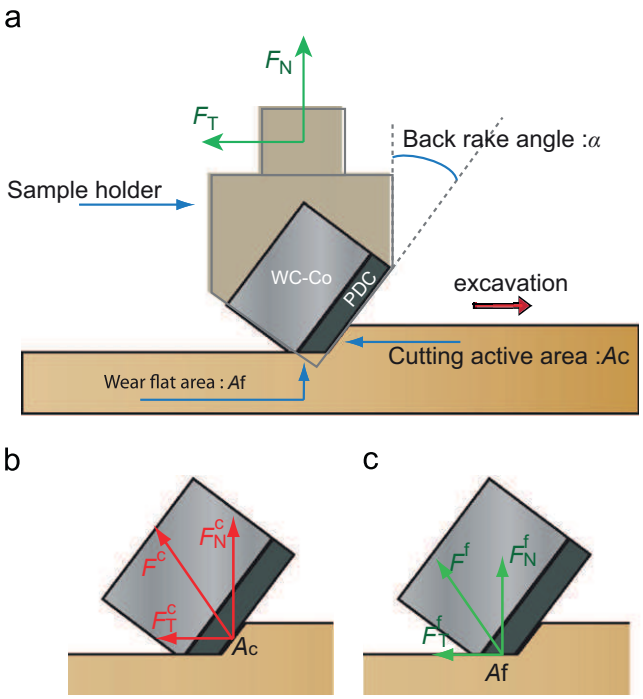

Fig. 4. Schematics of cutter/rock mechanical interactions: (a) overall cutter disposition; (b) cutting components; (c) friction components.

Table 2
Cobalt mean content and migration parameters obtained by EDX profiles analyzes for samples A to F (measurements of cobalt content exclude leached fields).

Cutters	A	B	C	D	E	F
Co wt.% in Diamond	2.9 ± 0.3	2.9 ± 0.8	2.7 ± 0.4	3.5 ± 0.4	3.4 ± 0.2	3.2 ± 0.2
Co wt.% in WC-Co	8.2 ± 0.2	16.7 ± 0.2	9.8 ± 0.2	11.2 ± 0.2	9.6 ± 0.1	7.7 ± 0.1
$\sqrt{D \cdot t}$ (mm)	0.2 ± 0.2	0.8 ± 0.1	0.5 ± 0.1	0.1 ± 0.1	0.3 ± 0.1	0.1 ± 0.1
x_i (mm)	3.0 ± 0.1	3.3 ± 0.2	2.7 ± 0.1	2.4 ± 0.1	2.6 ± 0.1	2.8 ± 0.1

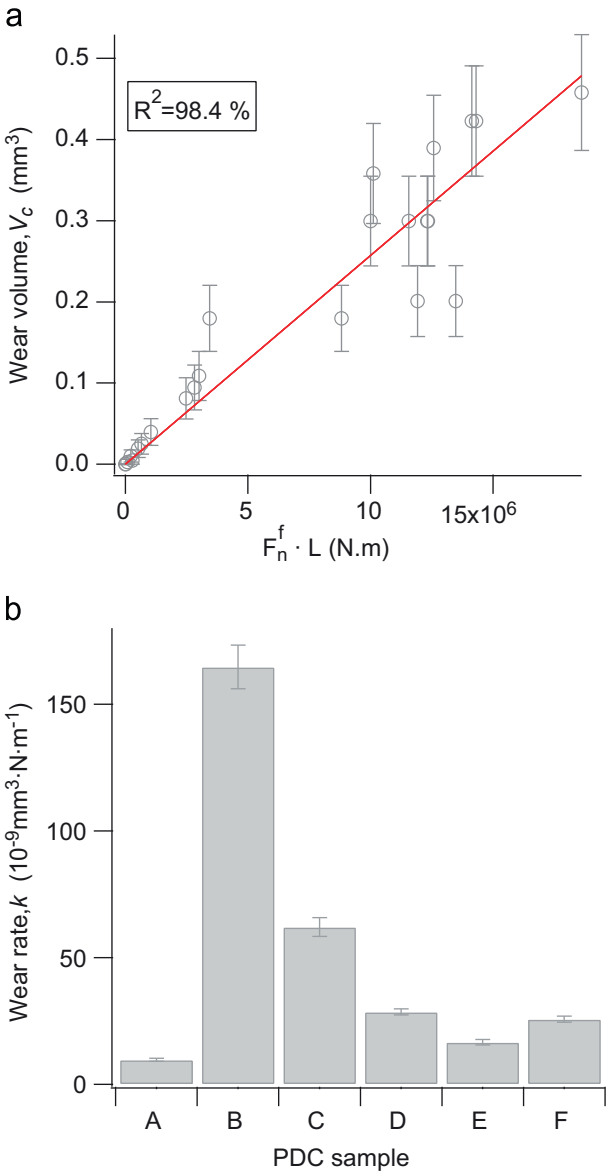

Fig. 5. Wear rate evaluation: (a) Archard's model applied to sample F; (b) wear rates results.

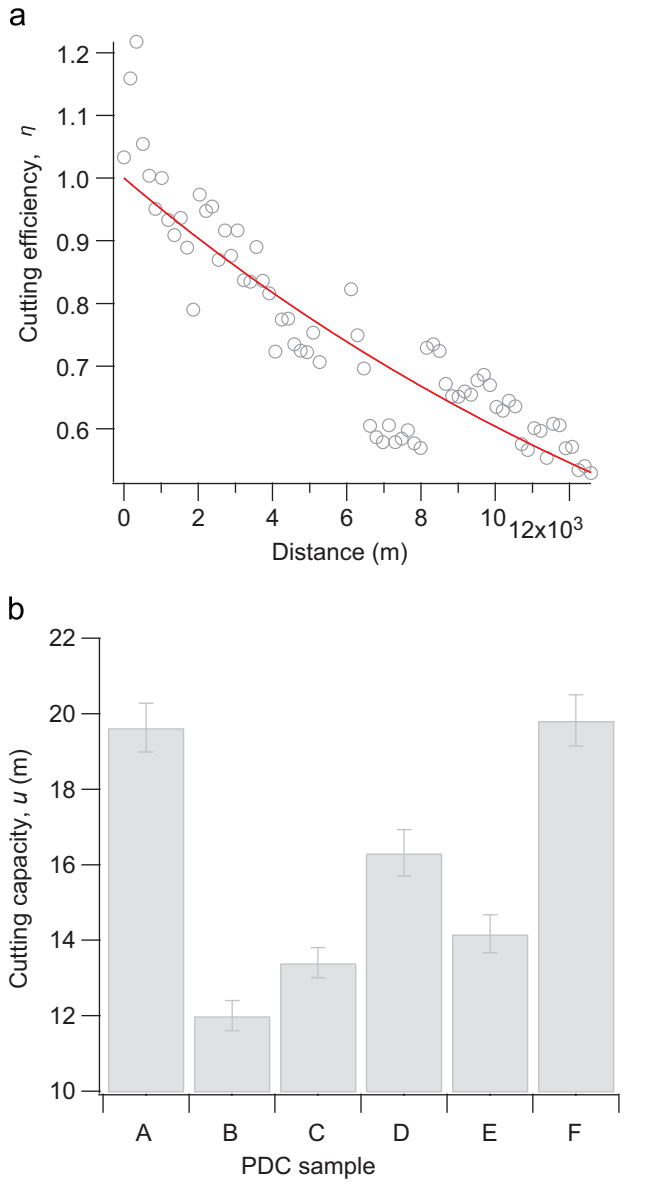

Fig. 6. Cutting efficiency analysis: (a) Cutting efficiency vs. distance model for sample F; (b) cutting capacity results.

specific energy calculations (Eq. (6))

$$E = \frac{E_m}{V_R} = \frac{F_T}{A_c} = \mu \frac{F_N}{A_c} + (1-\mu\zeta)\varepsilon \tag{6}$$

The ratio between ε and E characterizes drilling process efficiency η, which represents the cutting part in the overall mechanical action. Eventually, a pure cutting process means that $\mu = 0$ then $E = \varepsilon \approx E_0$ where E_0 is the initial value of E (Eq. (7))

$$\eta = \frac{\varepsilon}{E} = \frac{E_0}{E} \tag{7}$$

For all cutters, experiments revealed that cutting efficiency η plotted as a function of distance L follows a decreasing and nonlinear curve (Fig. 6a). When excavation test starts, η is closed to 1 (new cutter fully efficient) and as expected, η tends to 0 when the distance L becomes greater (mathematically infinite). The experimental cutting efficiency η can reach values higher than 1 at the beginning of the test, but these values are due to fluctuations in rock homogeneity and transitory periods occurring before cutting process stabilization. Accordingly, an exponential law as a function of excavating distance seems adequate to empirically evaluate the relative cutting efficiency behavior for each series of PDC samples. A constant coefficient u, expressed in meters, is introduced here and is identified as "cutting capacity" (Eq. (8))

$$\eta = \exp\left(-\frac{L}{u}\right) \tag{8}$$

The lowest value of cutting capacity u of 12 km was measured with B and the highest value around 20 km was obtained with A and F cutters (Fig. 6b).

6. Quality model

Obviously, separate analyzes of wear endurance and cutting efficiency do not clearly discriminate the relative quality of cutters. The grade assessment of PDC samples depends on its tribological behavior (i.e. friction and wear), cutting efficiency and rock cutting resistance (i.e. intrinsic specific energy). A low wear

rate and a high cutting efficiency of the sample ensure a high quality cutter. In order to compare cutter performances, a quality criterion must involve both wear rate and cutting efficiency. For that purpose, we first consider the grinding ratio G, which is the ratio between rock wear volume V_R and cutter wear volume V_c. The grinding ratio is commonly used to estimate cutters resistance by abrasive wear. By combining previous equations, this ratio can be directly related to the parameters ε, μ, k and η (Eq. (9))

$$G = \frac{V_R}{V_c} = \frac{A_c L}{k \cdot F_N^f L} = \frac{\mu F_T^c}{\varepsilon k F_T^f} = \frac{\mu F_T^c}{\varepsilon k (F_T - F_T^c)} = \frac{\mu}{\varepsilon k}\left(\frac{F_T}{F_T^0} - 1\right)^{-1} = \frac{\mu}{\varepsilon k}\left(\frac{1}{\eta} - 1\right)^{-1} \quad (9)$$

By introducing the experimental cutting capacity parameter u, the grinding ratio can be expressed as follows (Eq. (10)):

$$G = \frac{\mu}{\varepsilon k}\left[\frac{1}{\exp\left(-\frac{1}{u}\cdot L\right)} - 1\right]^{-1} = \frac{\mu}{\varepsilon k}\left[\exp\left(\frac{L}{u}\right) - 1\right]^{-1} = \frac{\mu}{\varepsilon k}\left[\frac{L}{u} + \sum_{n=2}^{+\infty}\left(\frac{L}{u}\right)^n\right]^{-1} \quad (10)$$

From here, it is interesting to define the quality factor Q, which is a dimensionless value integrating all variations of cutting efficiencies η over travel distance L_T (Eq. (11)). This distance should be high enough to measure significant wear evolution on samples. L_T was set at 12 580 m for the six samples.

$$Q = \frac{\mu}{\varepsilon L_T}\frac{u}{k} \quad (11)$$

These results display the interest in confronting μ, ε, L_T, k and u parameters and evaluating the quality factor (Table 3). First, this definition of quality factor takes into account coefficients μ and ε. The friction coefficient μ is directly associated to the tribological system formed between the cutter, the rock and the debris. The intrinsic specific energy ε is more linked to the rock mechanical properties as compressive strength. These two coefficients highlight the contribution of PDC and rock properties in cutter quality. Then, the ration u on k proves the compromise between cutting efficiency η and wear rate k in the quality formula. During experiments, rock inhomogeneities and contact variations can influence wear kinetic which affects the performance assessment of a cutter. Therefore, factor quality Q normalizes wear behavior with regard to dissipated energy during the cutting process. Eventually, Q is inversely proportional to L_T which is fixed for all tested samples. This comment only expresses that for higher excavation distances, cutters need higher cutting capacity and wear resistance to be qualified as good. That is why the quality factor depends on the targeted excavation distance.

According to quality factor results (Fig. 7), cutter A is clearly the best one with a Q factor about 169×10^4, which is confirmed by its low wear rate and its high cutting efficiency. In contrast, the cutter B registers the worst Q factor of only 4×10^4.

Four parameters influence cutter behavior: the amount of cobalt in the diamond table, the diamond grain size distribution, residual stresses and defaults (inclusions, cracks or porosities).

Cobalt ductile phase is directly associated to wear kinetic and the higher the cobalt proportion, the easier the abrasion of a drilling tool. In other words, master cobalt distribution in diamond permits to handle tools wear resistance. In this study, cobalt content differences in diamond parts are not significant and no rank can be made in relation with cobalt changes in samples. In addition, leached samples can not be discriminated from non-leached samples by the quality factor defined here. Cutters D, E and F are made by the same manufacturer and the leached depth is the only parameter differentiating them. Samples E and F are leached on less than 400 μm depth which corresponds to 20% of diamond layer thickness. Leaching depths represent respectively 14% and 40% of the final worn diamond thicknesses of samples E and F. This could explain the low influence of the leaching process on long excavation distances.

As seen above, cutters B and C may have a higher diamond grain size than others samples. These two cutters have the highest wear rates and lowest quality factors. As expressed by Bellin et al. [12], PDC cutters with a fine grain distribution are more resistant to abrasion than cutter with coarse grains. Nevertheless, it is an accepted fact that a coarse grain distribution permits a better impact resistance.

7. Phase analysis and quality factor

The samples were submitted to XRD (X-ray diffraction) measurements to study chemical differences between each diamond tables (Fig. 8). Diffractograms were recorded on a X'PERT Philips MRD diffractometer with CuK α radiation source beam at 40 kV and 50 mA. XRD measurements are also defined by 2θ Bragg angles from 10° to 160° with a step size of 0.02°.

Cobalt can exhibit three possible crystalline structures: hexagonal close packed α-Co phase, face-centered cubic β-Co phase and cubic also ε-Co phase [13]. In addition to diamond, two phases associated to cobalt element were identified on diffractograms: cobalt carbide (CoC_x) [14] and traces of cobalt (ε-Co) (Fig. 9).

As displayed on diffractogram of WC-Co part, the substrate contains only ε-Co phase. During sintering, cobalt elements migrated from WC-Co substrate towards PDC. This process explains the detection of ε-Co phase in diamond table.

The cobalt carbide phase is formed during sintering of PDC material. Thus, cobalt cannot be seen as a catalyzer of diamond formation but only as a precursor because it forms a new product with carbon. Actually, Akhaishi et al. [15] described the cobalt action during sintering as follows:

Table 3
Summary of mechanical results for samples A to F at $L_T = 12\,580$ m.

PDC samples	μ	ε (10^6 J m^{-3})	k (10^{-9} mm^3 N^{-1} m^{-1})	u (km)	Q (10^4)
A	0.261 ± 0.007	24.9 ± 0.8	9.6 ± 0.6	19.6 ± 0.6	169 ± 5.4
B	0.196 ± 0.004	30.4 ± 0.9	164.7 ± 8.6	12.0 ± 0.4	4 ± 0.1
C	0.218 ± 0.005	30.0 ± 0.8	62.0 ± 3.7	13.4 ± 0.4	12 ± 0.4
D	0.234 ± 0.005	25.5 ± 0.7	28.5 ± 1.2	16.3 ± 0.6	41 ± 0.4
E	0.230 ± 0.011	28.4 ± 1.5	16.6 ± 1.1	14.2 ± 0.5	55 ± 2.0
F	0.210 ± 0.011	29.1 ± 1.2	25.7 ± 1.2	19.8 ± 0.7	44 ± 0.2

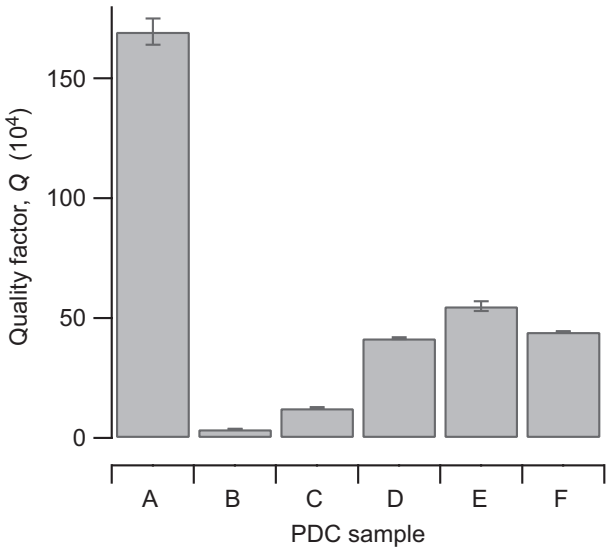

Fig. 7. Quality factors results with $L_T = 12\,580$ m.

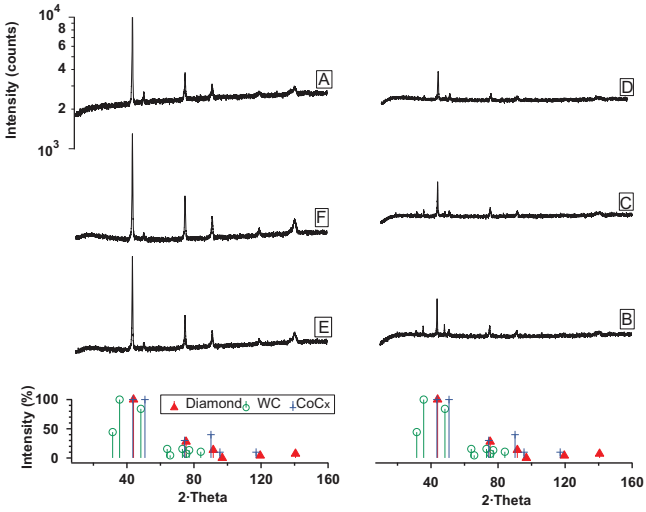

Fig. 8. Diffractograms of PDC samples A, B, C, D, E and F classified from low Q (sample B) to high Q (sample A) and calculated stick pattern of diamond, tungsten carbide and cobalt carbide.

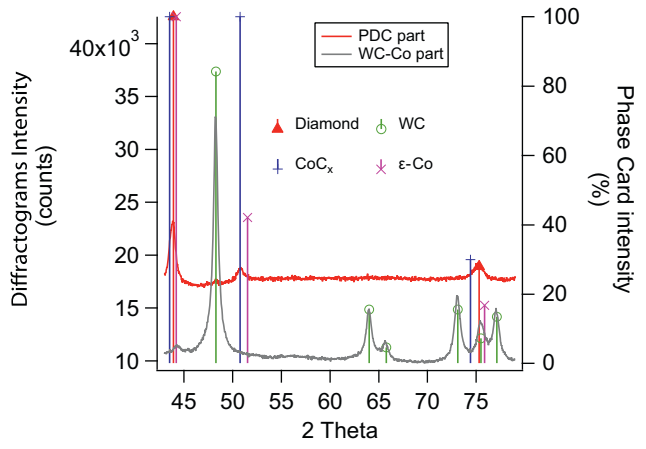

Fig. 9. Cobalt allotropic phases: sample D diamond and WC-Co parts diffractograms.

- At first graphite, formed on diamond grain surfaces at high temperature, dissolves into cobalt liquid phase above eutectic until saturation.
- From saturation, diamond precipitates and dissolution can start again until saturation of pure diamond into cobalt.
- Therefore, diamond grain size grows, densification increases by Oswald ripening and cobalt carbide appears in grain boundaries.

Like diamond, cobalt carbide is a metastable phase at room temperature. For example, Ishida and Nishizawa [16] note that, over a pressure of 4.5 GPa, Co_3C becomes a stable phase which corresponds to a lower pressure than requires synthetic diamond sintering conditions.

XRD peak intensity ($I_{diamond}$, I_{CoC_x} or I_{wc}) depends on the concentration of the identified crystallized phase. Also, diffracted X-rays by diamond grains are modified by the amount of absorbent cobalt phases surrounding them. Cobalt element has a higher atomic number than carbon element and likewise absorption coefficient. Thus, X-rays penetrate deeper in leached samples than non-leached ones. This explains the higher intensities measured for leached samples A, E and F. In addition, an interesting way to display relative proportions of phases in the PDC material consists to calculate the ratio between maximum peak intensity of the studied phase and the sum of maximum peak of all present phases (I) in the sample (Table 4). This calculation only leads to relative results because the phase attenuation coefficients are not taken into account [17]. As expected, the results obtained here show that the leaching process eliminates the cobalt carbide phase. This reinforces the fact that, in PDC table, the matrix surrounding diamond grains is essentially made of cobalt carbide phase.

Tungsten carbide phase was detected in the diamond table on only samples B, C and D. Manufacturers well-know that WC grain pollution, accidentally introduced during pressing and sintering, can weaken diamond grain cohesion [18]. Sample B has clearly the greatest proportion of WC and this can explain its low Q value relatively to other samples.

8. Residual stresses and quality factor

Three-dimensional finite element analyzes were carried out to evaluate post-sintering residual stresses. The diamond/carbide interface designs of samples B, C and D (i.e. also E and F) are considered. All samples are supposed to be sintered at a temperature of 1380 °C under an isostatic pressure of 5.5 GPa [19]. Then, a drop in the temperature until 1000 °C is taken into account and pressure is maintained to pass the solidus of the carbide part. Eventually, a last cooling is assumed until 20 °C at atmospheric pressure. Physical properties used for numerical simulations are identical (Table 5). To perform numerical simulations, the software Abaqus was used considering a steady state calculation and a tetragonal mesh of 0.5 mm size.

Radial, axial and shear stresses are calculated at the end of a simulation. Negative values of stresses are related to compressive state and positive ones to traction. Residual stresses are expressed relatively to the maximum traction values in radial, axial or shear directions obtained with a flat interface design. This approach

Table 4
Calculus of relative proportion of cobalt carbide and tungsten carbide in PDC samples A to F.

PDC samples	A	B	C	D	E	F
I_{CoC_x}/I	3.5 ± 0.9	7.9 ± 0.7	8.1 ± 0.6	11.4 ± 0.9	0.9 ± 0.9	0.7 ± 0.4
I_{WC}/I	–	16.4 ± 0.9	6.8 ± 0.7	8.3 ± 1.1	–	–

Table 5
Physical properties of PDC and WC-Co [20].

Material	Density ($kg\ m^{-3}$)	Thermal conductivity ($W\ m^{-1}\ K^{-1}$)	Specific heat ($J\ kg^{-1}\ K^{-1}$)	Thermal expansion coefficient ($10^{-6}\ K^{-1}$)	Young's modulus (GPa)	Poisson ratio
PDC	3510	543	790	2.5	890	0.07
WC-Co	15 000	100	230	5.2	579	0.22

Table 6
Residual stress distributions for flat interface design, samples B, C and D (i.e. also E and F).

	Radial stress distribution	Axial stress distribution	Shear stress distribution
Flat	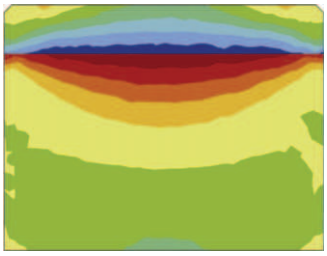		
B			
C	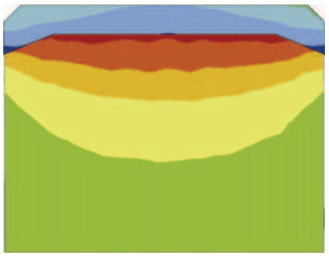		
D	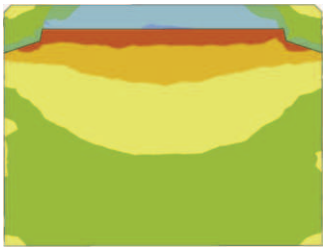		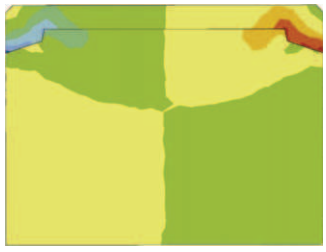

avoids numerical calibrations and considers only changes in stress distributions and amplitudes comparatively to the simple flat interface (Table 6).

The high traction residual stresses favor cracks propagation in grain boundaries and lead to diamond grain decohesion. The change in thermal expansion coefficient between WC-Co and diamond induces an overall cap-like radial stress distribution in compression in the PDC table and in traction in the substrate. This distribution was well illustrated by cap type cracks in the diamond part in several microsections performed by electroerosion (Fig. 10a). The radial stresses produce compressive field lines in the PDC material (Fig. 10b) and the addition of traction axial stresses can cause cap-like crack propagation guided by these field lines.

Simulation results indicate that the flat interface between diamond and WC-Co shows the highest gradient of residual stresses. At the interface, the radial stresses are compressive in the diamond and are symmetrically in traction in the substrate at respectively −100% and 100% by definition. In addition, the radial stresses reach more than 40% of the maximum traction value in localized zones on the diamond front face. The axial stresses exceed 60% on the perimeter and in the middle of the PDC table. Maximum axial values are compressive in the edge of the carbide part and tensile in the heart of this part. Most of the shear stresses is concentrated at the interface and reaches 60% (or symmetrically −60%) near the cylindrical edge of the sample. These considerations justify the work of manufacturers in trying to avoid traction field at the tip of a cutter by performing more

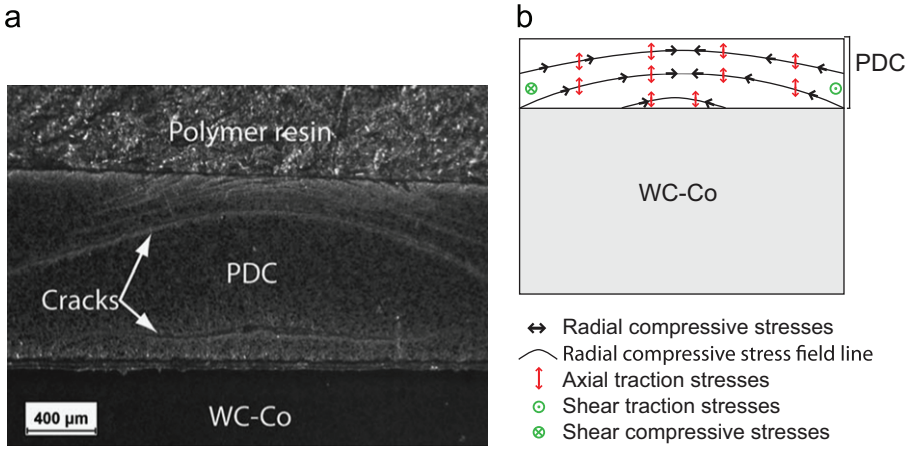

Fig. 10. Cap type crack formation: (a) cap type cracks observed on a microsection realized by electroerosion; (b) illustration of radial, shear and axial stresses actions in the PDC part.

complex interface designs. Indeed, all the studied designs modify the distribution of residual stresses and reduce traction fields compared to the flat interface.

The sample C reveals a diamond table with the highest compressive state (around -40%) in the radial direction. The substrate part counterbalances with high traction values (higher than 60%) near the interface. As the other manufacturers' designs, axial stresses are lightly in traction in the middle of the PDC part ($<20\%$) and in compression until (up to -100%) at the edge of the sample. High traction shear stresses were calculated ($>60\%$) at the interface near the edge in the diamond.

The samples B and D register a distribution of radial stresses less contrasted than sample C. Traction does not exceed 60% and compression is lower than -60%. Sample D has low radial traction fields ($<20\%$) at the tip of the diamond part. The samples B and D have also high axial stress concentration zones ($>60\%$) well localized at the interface angularities or waves in the WC-Co part. It is also interesting to note that sample B distributes traction shear stress in the two materials with regards to undulating design.

Eventually, considering abrasion resistance, the sample C has the most efficient design that permits a high compressive state at the sample tip compared to the other samples. This sample is followed by the cutter B in terms of compressive values in diamond. However, as seen above, these cutters have the worst quality factor results. Hence, residual stresses have to be considered with respect to cutters performances but diamond grain sizes have more significant impact on the relative quality of the six cutters. The edge of sample A is based on the same interface as sample D but it has a more complex design in the center. As sample B, the complex design along the interface permits to distribute residual stresses in the three directions. This enhancement of interface design could have contributed to the high quality factor estimated for the sample A.

9. Conclusion

A comparison among various PDC cutters submitted to wear tests requires an overlap of information. The PDC cutters assessment tends to balance ability to withstand abrasive wear and to remain efficient as long as possible. For this purpose, a quality factor was proposed as the ratio of the cutting capacity on wear rate multiply by coefficients associates to the cutter/rock contact. To determine the cutting capacity, an exponential law was fitted to the cutting efficiency decreasing with the excavation distance.

Four factors influencing the quality of cutters have been highlighted in this study:

- The diamond grain size distribution is the most sensitive parameter toward cutters abrasive resistance. As already expressed in previous studies and confirmed here, the finest diamond grains are the more abrasive resistant cutters.
- The cobalt element is a precursor of diamond formation and not a catalyzer, because cobalt carbide remains after PDC sintering. The increase of cobalt content in the diamond part increases samples wear rates. However, depleting cobalt on few hundred micrometers has not a significant effect on quality factor when long distance tests are performed.
- Low quality cutters contain tungsten carbide particles in diamond part.
- Traction residual stresses in diamond promote cracks propagation and induce lower abrasion resistance by weakening grain boundary.

Acknowledgment

This work was performed under the program ANR-09-MAPR-0009 of Agence Nationale de la Recherche. We thank Armines Geosciences laboratory for performing the wear experiments and the Varel Europe Company for providing cutters used in this study.

References

[1] J.L. Wise, D.W. Raymond, C.H. Cooley, K. Bertagnolli, Effects of Design and Processing Parameters on Performance of PDC Drag Cutters for Hard-Rock Drilling, Technical Report, Sandia National Laboratories, 2002.
[2] A. Ersoy, M. Waller, Wear characteristics of PDC pin and hybrid core bits in rock drilling, Wear 188 (1995) 150–165.
[3] A.K. Wojtanowicz, E. Kuru, Mathematical modeling of PDC bit drilling process based on a single-cutter mechanics, Journal of Energy Resources Technology 115 (4) (1993) 247–256.
[4] H.P. Bovenkerk, F.P. Bundy, H.T. Hall, H.M. Strong, R.H. Wentorf, Preparation of diamond, Nature 184 (1959) 1094–1098.
[5] N.D. Griffin, P.R. Hughes, High volume density polycrystalline diamond with working surfaces depleted of catalyzing material, United States patent US 6,562,462 B2 2003.
[6] J. Crank, The Mathematics of Diffusion, Oxford University Press, 1956.
[7] S.-M. Hong, M. Akaishi, H. Handa, T. Osawa, S. Yahmaoka, Behaviour of cobalt infiltration and abnormal grain growth during sintering of diamond on cobalt substrate, Journal of Materials Science 23 (1988) 3821–3826.
[8] D.A. Glowka, Development of a Method for Predicting the Performance and Wear of PDC Drill Bits, Technical Report, Sandia National Laboratories, 1987.
[9] L. Gerbaud, S. Menand, H. Sellami, PDC bits: all comes from the cutter rock interaction, in: IADC/SPE Drilling Conference, Miami, États-Unis, 2006, p. 1.

[10] C. Fairhurst, W. Lacabanne, Some principles and developments in hard rock drilling techniques, in: Sixth Annual Drilling and Blasting Symposium, 1956, pp. 12–25.
[11] E. Detournay, P. Defourny, A phenomenological model for the drilling action of drag bits, International Journal of Rock Mechanics & Mining Sciences and Geomechanics 29 (1992) 13–23.
[12] F. Bellin, A. Dourfaye, W. King, M. Thigpen, The current state of PDC bit technology, World Oil (2010) 41–46.
[13] V.A. de la Pena O'Shea, I.P.R. de Moreira, A. Roldan, F. Illas, Electronic and magnetic structure of bulk cobalt: the alpha, beta, and epsilon-phases from density functional theory calculations, The Journal of Chemical Physics 133 (2) (2010) 024701.
[14] A. Badzian, A. Klokocki, JCPDS-ICDD XRD card CoCx 00-044-0962, 1981.
[15] M. Akhaishi, H. Kanda, Y. Sato, N. Setaka, T. Ohsawa, O. Fukunaga, Sintering behaviour of the diamond–cobalt system at high temperature and pressure, Journal of Materials Science 17 (1982) 193–198.
[16] K. Ishida, T. Nishizawa, The C–Co (carbon–cobalt) system, Journal of Phase Equilibria 12 (1991) 417–424.
[17] R.P. Goehner, M.C. Nichols, X-ray powder diffraction-quantitative analysis, in: ASM Handbook, ASM International, 1986, pp. 693–695.
[18] Z. Qi, The manufacture of PDC for cutting tools, Science and Technology of New Diamond (1990) 415–416.
[19] T.N. Butcher, R.M. Horton, S.R. Jurewicz, S.E. Scott, R.H. Smith, Polycrystalline diamond cutters having modified residual stresses, United States patent US 6,220,375 B1, 2001.
[20] F. Chen, G. Xu, C. Ma, G. Xu, Thermal residual stress of polycrystalline diamond compacts, Transactions of Nonferrous Metals Society of China (2010) 227–232.